Damage Assessment of Reinforced Concrete Columns Under High Axial Loading

by S. Kono, H. Bechtoula, M. Sakashita, H. Tanaka, F. Watanabe, and M.O. Eberhard

Synopsis: Damage assessment has become more important than ever since structural designers started to employ performance based design methods, which require structural and member behaviors at different limit states be predicted precisely. This study aims to clarify the confining effect of concrete of a plastic hinge zone of a reinforced concrete column confined by shear reinforcement, so that a designer can accurately predict damage when columns experience seismic loadings that includes large axial force and bilateral deformations. In an experimental program, eight half-scale columns and eight full-scale columns were tested under the reversal bilateral displacement with constant or varying axial load in order to study the effects of loading history and intensity on the confining effect. Since shear failure was inhibited by providing enough transverse reinforcement, as defined by the previous Japanese design guidelines, damage gradually progressed in a flexural mode with concrete crushing and yielding of reinforcing bars. The damage level depended on the bilateral loading paths and the axial load history. In an analytical program, a section analysis using a fiber model was employed and the effect of confinement on the behavior of core concrete was studied. The analysis predicted the observed deterioration of moment capacity and longitudinal shortening under different loading conditions and for different specimen sizes. The study is considered to increase the accuracy with which damage in reinforced concrete columns subjected to severe loading is assessed.

Keywords: bilateral loading; confining effect; damage assessment; fiber model; high axial loading; plastic hinge; RC column; stress-strain relation of concrete

S. Kono is Associate Professor of the Department of Architecture and Architectural Engineering at Kyoto University, Japan. His research interests include the damage prediction of reinforced concrete structures for performance based design, histeresys characterization of prestressed concrete members, and evaluation of shear transfer at precast concrete interface.

H. Bechtoula earned his Ph. D. degree from the Department of Architecture and Architectural Engineering, Kyoto University, Japan. He is currently enrolled as a Ph. D. student at Kyoto University. His research interests include seismic design of reinforced concrete structures.

M. Sakashita holds M.S. degree from the Department of Architecture and Architectural Engineering, Kyoto University, Japan. He is currently enrolled as a Ph. D. student at Kyoto University. His research interests include seismic design of shear wall considering the interaction between superstructure and foundation.

H. Tanaka is Professor of Disaster Prevention Research Institute at Kyoto University, Japan. His research interests include the improvement of seismic design of buildings, including foundations. Fundamental studies have been carried out to elucidate the dynamic characteristics of building structures with various types of foundations.

F. Watanabe is Professor of the Department of Architecture and Architectural Engineering at Kyoto University, Japan. His research interests include shear problems, ductility enhancement, development of seismic design method for reinforced and prestressed concrete ductile frames, and high strength concrete.

M. O. Eberhard is Associate Professor of the Department of Civil and Environmental Engineering at the University of Washington. His research interests include seismic design and nondestructive evaluation of reinforced concrete structures.

INTRODUCTION

For a building structure to have a reliable beam side sway mechanism under seismic loading, one of the most critical sections is the hinge zone at the base of the lowest floor columns. They are subjected to high axial load variation with bilateral displacements under earthquake loadings. Although extensive studies have been done to predict the hysteretic behavior of column hinges, it is still difficult to correctly predict the damage progression such as cracking, crushing, and spalling of concrete, buckling of reinforcement, etc. Consequently, a method to assess damage and estimate the remaining capacity after earthquakes loading has not been established. Rao et al. (1998) and Park et al. (1985) proposed damage models but their models require use of a complete earthquake history. The authors proposed (Kono and Watanabe, 2001) a moment damage index $I(M)$ that can be computed from the maximum compressive strain demand. The moment damage index is defined in Eqs. (1) and (2) where the nomenclature is explained in Fig. 1.

$$I(M_x) = \frac{\int_A f_{\max} \cdot |y| \, dA}{\int_A f_{peak} \cdot |y| \, dA} \quad (1)$$

$$I(M_y) = \frac{\int_A f_{\max} \cdot |x| \, dA}{\int_A f_{peak} \cdot |x| \, dA} \quad (2)$$

where A is the area of the column section and x *and* y are the distances of infinitesimal area, dA, from the centroid of the section in x and y directions, respectively. Damage index, $I(M)$, was shown to simulate the degradation of concrete load carrying capacity with a good accuracy for specimens listed in Table 1 as shown in Fig. 2 where the strength reduction factor, Rc, is defined by Eq. (3) and computed based on the moment carried by the concrete:

$$Rc = \frac{Maximum\ moment\ value\ \ for\ each\ cycle}{Maximum\ moment\ value\ \ for\ whole\ history} \quad (3)$$

However, the usefulness of $I(M)$ largely depends on the accuracy of the simulated distribution of stresses and strains across the column cross section. If the simulation does not describe the realistic distribution of stresses and strains, the damage indices computed based on these quantities will not have high accuracy. Even if different damage indices are used, an accurate description of the stress state is required to enable evaluating damage in the plastic hinge zone. Hence, the behavior of concrete columns was studied using both experimental and analytical approaches. In this study, sixteen first-floor column-base models with a square section were tested under multi-axial reversed cyclic loading to investigate the sensitivity of the moment-curvature relations and axial shortening-curvature relations in the plastic hinge region to load path, axial force intensity, and specimen size. The hysteretic behavior of a plastic hinge was simulated using a simple fiber model and the importance of the concrete confining effect evaluating the stress state of core concrete in plastic hinge zones was clarified.

EXPERIMENTAL PROGRAM

Test set-ups

Sixteen cantilever column models with a square section as shown in Fig. 3 and Fig. 4 were tested under quasi-static bilateral displacements combined with different axial load levels in order to see axial load intensity, specimen size and load history on the behavior of a plastic hinge region. Numbers in parentheses under heading (a) for each figure indicate the specimen numbers in Table 1. The flexural failure of core concrete was designed to precede the shear failure in the plastic hinge zone by providing enough transverse reinforcement based on the current Japanese design guidelines (AIJ, 1997). The specimen was connected to a three-hydraulic jack system, which applied orthogonal

horizontal displacements at the top of the cantilever column. The representative specimen dimensions and test variables are listed in Table 1. Horizontal displacement patterns were linear, circular, and square and some of those paths are shown in Fig. 5(a) and (b). Intensity of axial force was either constant or varied proportional to the sum of moments $\mathcal{M}x$ and $\mathcal{M}y$ as shown in Fig. 5(c). The slope in axial force ($\mathcal{N}$) - moment ($\mathcal{M}$) relation is provided in Table 1. The axial load at the beginning of the test was half of the axial load variation. For example, D1NVA started from $0.3f'_c\mathcal{D}^2$ where the axial load varied between 0 to $0.6f'_c\mathcal{D}^2$.

Experimental results

All specimens showed ductile flexural behavior until the termination of loading. Visual observation showed that specimens with large axial force had more damage than those subjected to small axial force. The spalling of concrete cover was limited to the lower 0.5D region for small specimens and to the lower 1.5D region for larger specimens, where D is the column width.

Damage can be evaluated also from moment-curvature relation and axial strain-curvature relation as some selected results are shown in Fig. 6. The axial strain in the figures is the longitudinal strain at the centroid of the column section. The experimental axial strain and the curvature were taken as the mean values for the lower 1.0D region and moment was taken at the base of the column. From the figures, it can be seen that the moment-curvature relation was stable and did not degrade even well after the peak load. Application of large axial force, $0.6f'_c\mathcal{D}^2$, accelerated the shortening of columns as seen in Fig. 6(d) where axial strain is negative for shortening. However, specimens under low axial load or varying axial load did not show much shortening (Fig. 6(b)).

ANALYTICAL PROGRAM

Section analysis

Section analysis was carried out assuming Bernoulli's theory (plane section remains plane). The column cross section was subdivided into 576 concrete fiber elements (576=24x24) and 12 reinforcing steel fiber elements. Section response was computed by integrating all fiber element stresses and stiffnesses. Concrete fiber element follows Popovic's stress-strain relation as shown in Fig. 7(a). Steel fiber element follows the Ramberg-Osgood stress-strain relation as shown in Fig. 7(b). The peak point of the stress-strain relation of concrete is based on the study by Sakino and Sun (1994). The enhanced strength, f_{peak}, shown in Fig. 7(c) due to confinement is expressed as follows.

$$f_{peak} = f'_c + \kappa \rho_h f_{hy} \tag{4}$$

$$\kappa = 11.5\alpha\left(\frac{d}{C}\right)\left(1 - \frac{s}{2D_{core}}\right) \tag{5}$$

where f'_c is the cylinder compressive strength without confinement, κ, is the coefficient of strength enhancement due to confinement, ρ_h, f_{hy}, d, and C are the volume ratio, yield strength, diameter, and unsupported length of shear reinforcing bars, respectively, s is the distance between adjacent shear reinforcement, and D_{core} is the width of confined concrete core. The authors proposed a simple modification in the stress-strain relation. In Eq. (5), the coefficient, α, was inserted to the original equation to take into account the effects of strain gradient. An α value was taken greater than 1.0 to increase the strength and ductility of confined concrete as shown in Fig. 7(c). Without α, the analytical model gave moment capacities much lower than the experimental results.

In the analysis, α was varied so that the analytical results best fit the experimental results An assessment function, D_E, was defined as Eq. (6) for optimization. D_E represents the average error of axial strain normalized by ε_0 as shown in Fig. 8(a) where ε_i represents the difference between the experiment and the simulation at the i_{th} target point and ε_0 is expressed by Eq. (7). The target points were taken as the local maximum or local minimum points for each hysteretic loop of the moment-curvature relation and each specimen had 12 to 50 target points depending on the number of loading cycles. Variation of D_E with respect to α for L1D60 is shown in Fig. 8(b) as an example. The optimal α values for all specimens are listed in Table 2.

$$D_E = \frac{1}{n}\sum_{i=1}^{n}\left|\frac{\phi_i}{\phi_0}\cdot\frac{\varepsilon_i}{\varepsilon_0}\right| \tag{6}$$

$$\varepsilon_0 = \frac{2f'_c}{E_c} = \frac{2f'_c}{4730\sqrt{f'_c}} = \frac{\sqrt{f'_c}}{2365} \quad (f'_c \text{ in MPa}) \tag{7}$$

$$\phi_0 = \frac{2\varepsilon_0}{D} \tag{8}$$

Analytical results

The simulated moment-curvature relations and axial strain-curvature relation are compared with experimental results and some of them are shown in Fig. 6. The optimization of α is considered reasonable.

Table 2 shows some interesting facts. First, specimens with higher axial force have higher α, for example, from comparisons of D1N30 and D1N60 or D2N30 and D2N60. Specimens with axial load that varied between 0 and $0.6f'_cD^2$ have similar α values to specimens with constant axial force of $0.3f'_cD^2$. This shows that the axial force needs to be considered as one of major sources of constraint that enhances the ductility and strength of confined concrete. Second, specimens with bilateral loading condition have higher α values than those with linear loading condition. This can be seen, for example, from comparisons of D1N30 and D2N30 or D1N60 and D2N60. Third, small scale

specimens have higher α than full-scale specimens. This can be seen by comparing specimens with similar test variables except specimen size in the table.

Numerical study shows that the confining effect depends on axial load level, loading pattern in a horizontal plane, and specimen size. Here, the confining effect means the enhancement in axial strength and ductility of concrete due to lateral pressure. Generally, severe loading conditions cause more concrete damage and dilation of core concrete. The numerical analysis shows that this dilation is more effectively confined for smaller specimens leading to enhanced strength and ductility. Since ordinary beams have no axial force and have moment acting solely on one axis, the confining effect is smaller than for columns. However, ordinary columns have confinement enhanced by axial force and often bilateral bending, and this confining effect seems to have an important influence on the progression of damage in columns. In this sense, the corner columns of the ground level can expect the experience the greatest level confinement as the damage progresses. Although enhancing confining effect in concrete does not necessarily mean enhanced ductility in column as damage of concrete in the section needs to be integrated to obtain the behavior of column. However, the confining effect is considered a key to understanding of damage evaluation in reinforced concrete members.

CONCLUSIONS

Sixteen cantilever column specimens with a square section were tested under quasi-static bilateral displacements combined with different axial load level. The following conclusions were drawn from the experiments and analytical study.

- Degradation of moment capacity was small for a plastic hinge region when the specimens had enough confinement. However, even a high level of confinement did not stop longitudinal shortening under high constant axial load of $0.6f'_cD^2$. The longitudinal shortening did not progress very much for specimens with smaller axial loads.
- A simple fiber model with modified concrete confining effects was able to simulate observed moment-curvature relation and axial strain-curvature relations with good accuracy. The model proved that the confining effect was enhanced by severe loading conditions such as high axial loading and bilateral loading. It was also shown that smaller specimens enhanced the confinement more effectively than the larger specimens. With proposed α combined with Sakino's equation, more precise prediction of local damage on concrete and steel can be made in the design process.

ACKNOWLEDGMENT

The paper is based on the experiments and analyses conducted by T. Kuroyama, T. Ikeuchi, R. Fujimoto, N. Matsuishi, M. Ando, and I. Amemiya, all of whom were former students at Kyoto University. Sincere thanks are extended to Prof. T. Kaku and Prof. Kuramoto at Toyohashi University of Technology who gave us continuous support and suggestions through the experiment. The authors also acknowledge TOPY Industries

Limited, NETUREN Corporation Limited, KOBE Steel Limited for donating of experimental materials.

REFERENCES

1. Architecture Institute of Japan (1997). Design guidelines for Earthquake Resistant Reinforced Concrete Buildings Based on Inelastic Displacement Concept.

2. Kono S. and Watanabe F. (2001). Damage evaluation of reinforced concrete columns under multiaxial cyclic loadings. Proceedings of Concrete under severe conditions: environment and loading: 1947-1954.

3. Kono S., Arai, Y., Bechtoula, H., and Watanabe, F. (2002). Damage evaluation of reinforced concrete columns under large axial load and lateral deformation. Proceedings of the first FIB congress 2002, Vol. 1, Session 6 (2002): 65-66.

4. Kono S.， Arai Y.， Bechtoula H., and Watanabe F. (2003). Damage assessment of reinforced concrete columns under high axial loading. International Conference on Performance of Construction Materials, Cairo， Vol.1: 291-300.

5. Park, Y. J., Ang, A. H. S., and Wen, Y. K., (1985). Seismic Damage Analysis of Reinforced Concrete Buildings. Journal of Structural Engineering, ASCE, Vol. 111, No. 4: 740-757.

6. Rao, P. S., Sarma, B. S., Lakshmanan, N., and Stangenberg, F. (1998). Damage Model for Reinforced Concrete Elements under Cyclic Loading. ACI Materials Journal, Vol. 95, No. 6: 682-690.

7. Sakino, K, and Sun, Y. (1994). Stress-strain curve of concrete confined by rectilinear hoop. Journal of structural and construction engineering, Architecture Institute of Japan, No. 461: 95-104. (In Japanese)

Table 1 -- Test variables

No.	Specimen designation	Specimen configuration					Test Variables		
		Column width D (mm)	Shear span L (mm)	Concrete strength f'c (MPa)	Longitudinal rebar (ratio) [fy]	Shear rebar (ratio) [fy]	Axial force (Axial force level in $f'cD^2$)	Slope in moment-axial force relation (MN/MN・m)	Lateral loading directions (Trace)
1	D1N30	250	625	26.8	12-D13 2.44% 467MPa	$\bar{4}$@40 0.50% 604MPa	Constant (0.3)	0	Uni
2	D1N60						Constant (0.6)		
3	D2N30						Constant (0.3)		Bi (Circular)
4	D2N60						Constant (0.6)		
5	D1NVA	242		37.6	12-D13 2.60% 461MPa	$\bar{4}$@40 0.52% 485MPa	Varied (0 to 0.6)	5.7	Uni
6	D1NVB							11.5	
7	D2NVA							4.3	Bi (Circular)
8	D2NVB							6.9	
9	L1D60	600	1200	39.2	12-D25 1.69% 388MPa	D13@100 0.85% 524MPa	Constant (0.6)	0	Uni
10	L1N60								
11	L1NVA						Varied (0 to 0.6)	4.2	
12	L2NVA								Bi (Circ.)
13	L1D6B	560		32.2	12-D25 1.94% 388MPa	D13@100 0.91% 524MPa	Constant (0.6)	0	Uni
14	L2N60								Bi (Square)
15	L2NVB						Varied (0 to 0.6)	6.0	
16	L2NVC								

Table 2 -- Optimal value of α and D_E

No.	Specimen	Axis	α	Error D_E
1	D1N30	Uniaxial	2.2	0.16
2	D1N60	Uniaxial	4.3	0.47
3	D2N30	X	3.6	0.26
		Y	3.4	1.10
4	D2N60	X	8.4	0.21
		Y	7.8	0.29
5	D1NVA	Uniaxial	2.8	0.21
6	D1NVB	Uniaxial	1.6	0.24
7	D2NVA	X	4.6	0.29
		Y	2.8	0.28
8	D2NVB	X	3.0	0.80
		Y	2.6	0.38
9	L1D60	Uniaxial	3.2	0.71
10	L1N60	Uniaxial	3.0	0.38
11	L1NVA	Uniaxial	2.2	1.94
12	L2NVA	X	2.4	0.38
		Y	2.4	1.70
13	L1N6B	Uniaxial	1.0	0.95
14	L2N60	X	1.6	2.53
		Y	1.6	1.04
15	L2NVB	X	1.0	0.48
		Y	1.0	0.71
16	L2NVC	X	1.0	0.16
		Y	1.0	0.20

Note: Optimization was carried out for curvature about x axis - axial strain relation and curvature about y axis - axial strain relation independently for bilateral bending cases.

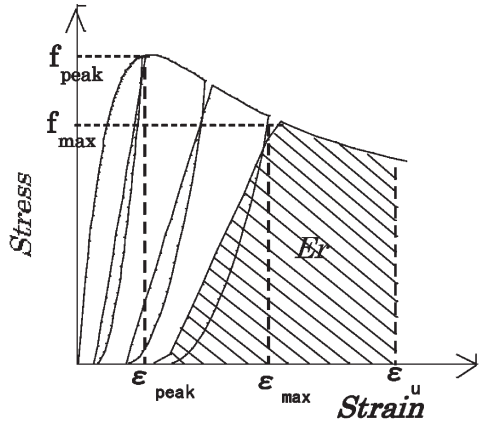

ε_{max}: maximum strain experienced

f_{max}: current attainable maximum stress

$f_{max} = f_{peak}$ for $\varepsilon_{max} < \varepsilon_{peak}$

f_{max} = stress corresponding to ε_{max} on the skeleton curve for $\varepsilon_{max} > \varepsilon_{peak}$

f_{peak} = maximum concrete strength considering confining effect

ε_{peak} = strain corresponding to f_{peak}

ε_u = ultimate strain considering confinement

Fig. 1 -- Stress-strain relation of concrete

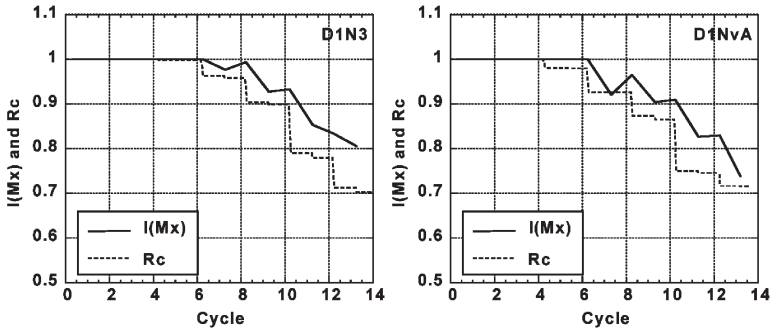

(a) Specimen D1N3 (b) Specimen D1NVA

Fig. 2 -- Comparison between the proposed damage index, $I(Mx)$, and the concrete contribution to moment, Rc

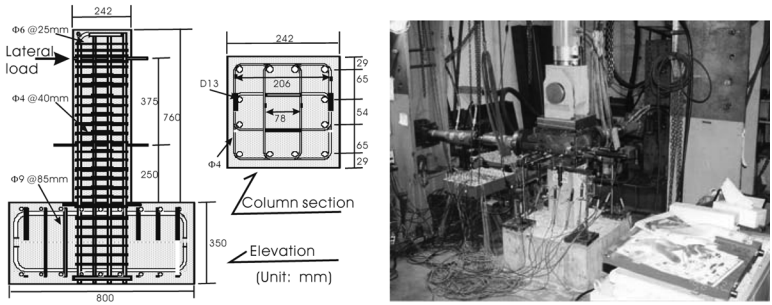

(a) Reinforcement configurations (No.5 – No.8). (b) Loading system

Fig. 3 -- Specimen dimensions and loading system for small specimens

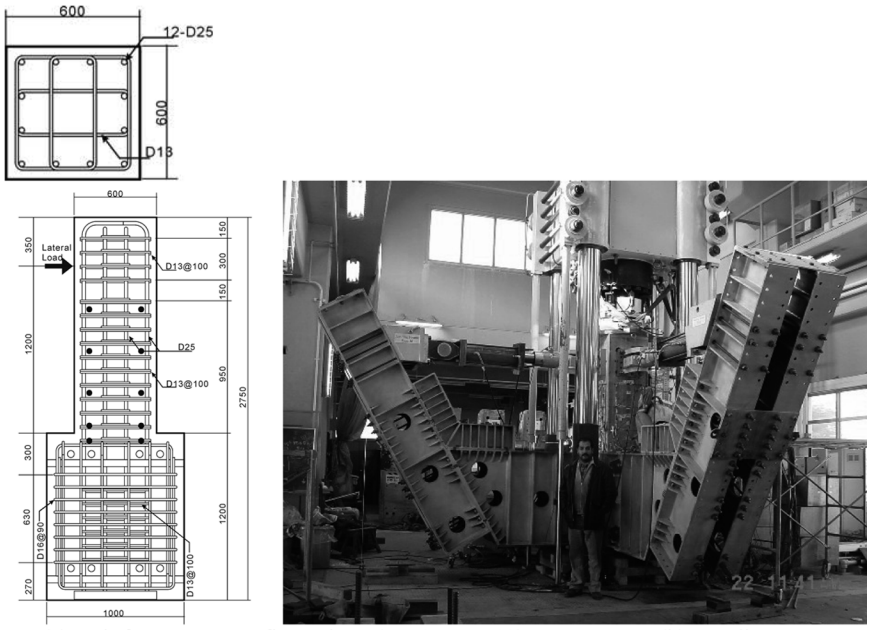

(a) Reinforcement configurations (No.9 – No.12). (b) Loading system

Fig. 4 -- Specimen dimensions and loading system for large specimens

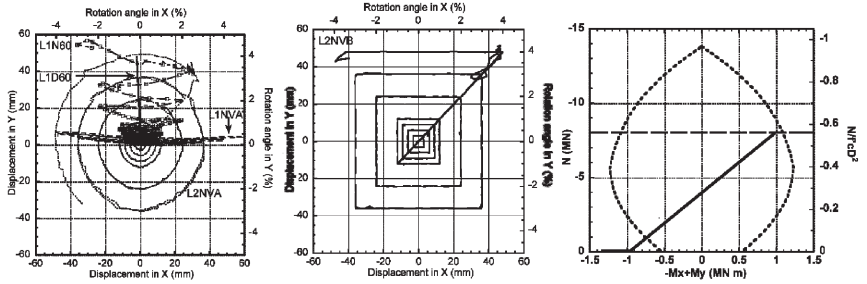

(a) Circular path (b) Square path (c) Path in N-M relation

Fig. 5 -- Loading pattern example

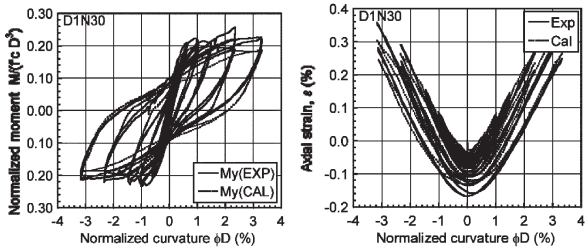

(a) Moment for D1N30 (b) Axial strain for D1N30

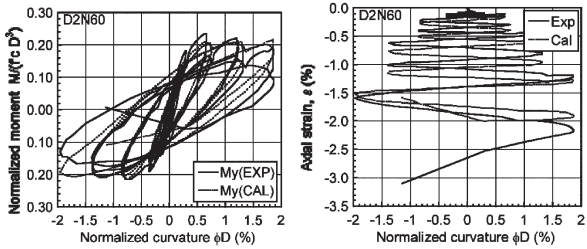

(c) Moment for D2N60 (d) Axial strain for D2N60

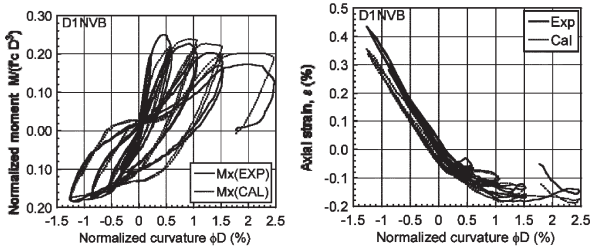

(e) Moment for D1NVB (f) Axial strain for D1NVB

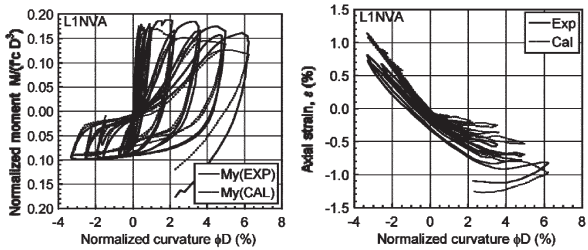

(g) Moment for L1NVA (h) Axial strain for L1NVA

Fig. 6 -- Four representative cases showing difference between test results and predictions using α in Table 2

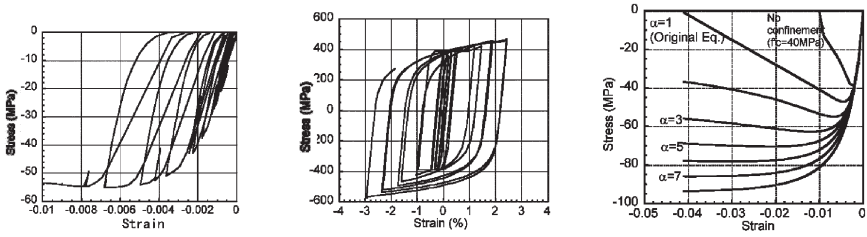

(a) Concrete (b) Steel (fy=388MPa) (c) Effect of α on the envelope

Fig. 7 -- Stress-strain relations

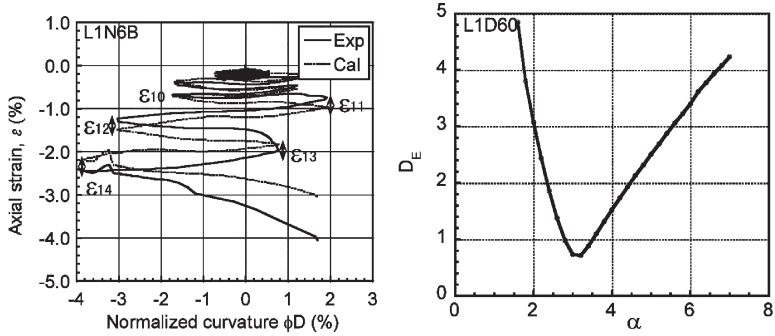

(a) Axial strain - curvature relation (b) D_E - α.relation (L1D60)

Fig. 8 -- Definition of error, ε_i, and variation of D_E in terms of α